Supplemental Data

Cell, *Volume 133*

Capping Protein Increases the Rate of Actin-based Motility by Promoting Filament Nucleation by the Arp2/3 Complex

Orkun Akin and R. Dyche Mullins

Supplemental Discussion

At the highest ratios of CP to Arp2/3, the actin networks become too inhomogeneous to support efficient steady-state motility or shell growth. MovieS5 demonstrates two defining features of this concentration regime: (1) The actin network does not remain connected around the bead. (2) Patches of the network frequently lose contact with the surface and float away. We attribute the loss of network connectivity mainly to the decrease in average filament length. These networks are not held together by traditional crosslinking proteins that can link any two filaments, regardless of their origin. They are, instead, entangled arbors of branched filaments. The degree of entanglement will increase with both the density of Arp2/3 branches and the average length of the filaments. While the density of branches is high at high CP concentrations, we suspect that the average filament becomes too short to connect isolated dendritic arbors. As a result, the ActA-coated beads generate disconnected fragments of network that never coalesce into a coherent shell. The second feature, loss of contact with the bead surface, is likely a symptom of limiting Arp2/3: In our study of steady-state motility and shell growth, we were constrained to concentration ranges that produced actin structures robust enough to be characterized with our current methods. It is within these ranges that we found the rate of nucleation to increase with CP concentration independent of the Arp2/3 concentration. Of course this trend can not continue indefinitely, and we believe that the network dynamics at higher CP to Arp2/3 ratios reflect the effects of limiting Arp2/3 concentrations. In our system, the Arp2/3 complex is one of two possible modes of surface:network attachment, the other being the WH2 domains of the immobilized NPF (Co et al., 2007). Thus, if the assembly process has to 'wait' for new Arp2/3 complexes to arrive at the bead surface, i.e. when Arp2/3 is limiting, the actin network frequently loses contact with the surface altogether.

Supplemental Experimental Procedures

Protein Purification and Modification

Cytoplasmic actin was purified from *Acanthamoeba castellani* by the method of Gordon et al. (1976). Actin was stored in 0.5 mM TCEP, 0.1 mM $CaCl_2$, 0.2 mM ATP, 2 mM Tris [pH 8.0] and gel filtered before use. Arp2/3 was prepared from *Acanthamoeba castellani* by the method of Dayel et. al. (2001) and further purified by cation exchange chromatography on monoS (GE Healthcare). Recombinant mouse CP $\alpha1\beta2$ was purified as described (Palmgren et al., 2001). Recombinant *Acanthamoeba castellani* cofilin (i.e. actophorin) was purified as described (Quirk et al., 1993). Recombinant human profilin I was purified by poly-L-proline affinity chromatography as described (Kaiser et al., 1989). Full-length *Listeria monocytogenes* ActA lacking the signal sequence and membrane anchor, $ActA^{30-612}$, was extended at the C-terminus with a KCK motif and a 6xHis-tag using standard molecular biology techniques. (Primer information is available upon request.) $ActA^{30-612}$-KCK-6H was expressed in *E.coli* and purified on Ni-NTA resin (Qiagen) under denaturing conditions followed by anion exchange chromatography on monoQ (GE Healthcare). The minimal Arp2/3-activating domain of ActA, $ActA^{30-170}$, (Zalevsky et al., 2001) was extended at the C-terminus with a 6xHis-tag using standard molecular biology techniques and purified as $ActA^{30-612}$-KCK-6H. Actin was labeled on Cys-374 with tetramethylrhodamine-maleimide (Invitrogen) as described (Otterbein et al., 2001). Essentially the same protocol was used to label actin with Alexa488-maleimide (Invitrogen), except the labeled protein was recovered in the polymerized actin pool. Arp2/3 was labeled with Alexa488-maleimide as described (Zalevsky et al., 2001).

Motility Assays and Microscopy

Carboxylated polystyrene beads were purchased from Bangs Labs. Except for the aster shown in Supplemental Figure 3, all experiments were carried out with beads coated with the $ActA^{30-612}$-KCK-6H construct, referred to

as 'ActA' in the text. ActA was covalently crosslinked to the beads using EDC:sulfoNHS (Pierce) chemistry. Briefly, bead suspensions corresponding to 10^{10} μm^2 /mL of surface area were charged with EDC in the presence of sulfoNHS. Beads were washed to remove excess crosslinker and coupled to 2-4 μM ActA for 2 hours at room temperature. Non-specifically adsorbed protein was removed by washing the beads in buffer containing 0.1% NP-40 and 2 M urea. The efficiency of crosslinking was determined by quantifying the ActA concentration in the flow-through and subsequent washes using fluorescently-stained SDS gels. The calculated surface density of crosslinked ActA varied between $2x10^4$ and 10^5 μm^{-2} and correlated with the bead-specific density of functional groups reported by the manufacturer. The final product was stored in 1 mg/mL BSA, 2 mM Tris [pH 8.0] and used at 1:30 dilution in motility assays.

All images were acquired on a software-controlled (SimplePCI, Compix) Nikon TE300 Eclipse inverted epifluorescence microscope equipped with a digital camera (Model C4742-98, Hamamatsu). To minimize non-specific protein adsorption, glass slides (Fisher) and coverslips (Corning) were washed in ethanol and KOH and treated with a 2% solution of diethyldichlorosilane (Gelest) in 5% water, 95% isopropanol [pH 4.5 with acetic acid]. Microscopy chambers were prepared by spreading 1-5 μL of motility mix between the glass pieces. To prevent evaporation, the chambers were sealed with valap (molten mixture of vaseline, lanolin, and paraffin at 1:1:1 mass ratio).

Biochemical Analysis of Shell Growth

Shell growth reactions set up with 3 μM actin were arrested by diluting 1:1 into KMEI (50 mM KCl, 1 mm MgCl2, 1 mM EGTA, 10 mM imidazole [pH 7.0]) containing 20 μM each of Latrunculin B and phalloidin. Shells in the arrested reactions were sedimented at 500 rcf for 2 minutes. Pelleted shells were washed three times using a magnetic separator and resuspended within 12 minutes of arrest. Bead density in the resuspended samples was determined using a hemocytometer. Supernatants from the low speed spin were spun again at 360 K rcf for 15 minutes. Dilution series of the original reactions, washed shells, and high speed pellets and supernatants were run on 4-12% tris-glycine gels (Invitrogen). The gels were stained with Sypro Ruby (Invitrogen), imaged with a Typhoon 9400 fluorescence imager (GE Healthcare), and analyzed using ImageQuant (GE Healthcare).

Image Analysis

Distances traveled by motile comet tails were determined by tracking the centroids of binarized phase-contrast bead images. Comet tail lengths were measured using skeletonized binary masks from fluorescence images. Shell sizes were measured using a routine that accepted user corrections to initial estimates based on intensity statistics. Image intensity adjustments for figures were performed with Photoshop (Adobe) and ImageJ (http://rsb.info.nih.gov/ij/). Unless noted otherwise, the intensity adjustment of each image was performed independently of accompanying images in the same figure.

Calculation of Elongation Rates

Actin assembly during shell growth can be described by the equation $d/dt[P] = k_+[A][E]-k_-[E]$, where [P] is the concentration of filamentous actin in shells, [A] is the concentration of monomeric actin, [E] is the concentration of free barbed ends, and k_+ and k_- are the kinetic constants for the interaction of actin monomers with barbed ends. The net elongation rate per barbed end, $k_+[A]-k_-$, is dominated by k_+. To estimate the value of k_+ during shell growth, we evaluated the time-sum form of the rate equation, using the measured values of [P] and [A], the estimated value of [E], and the published value of k_- (Pollard, 1986). We solved for k_+ over each interval of the experimental time series. Values shown in Supplemental Figure 6C are each the average of four estimates, corresponding to separate solutions over four time intervals.

Supplemental Figures

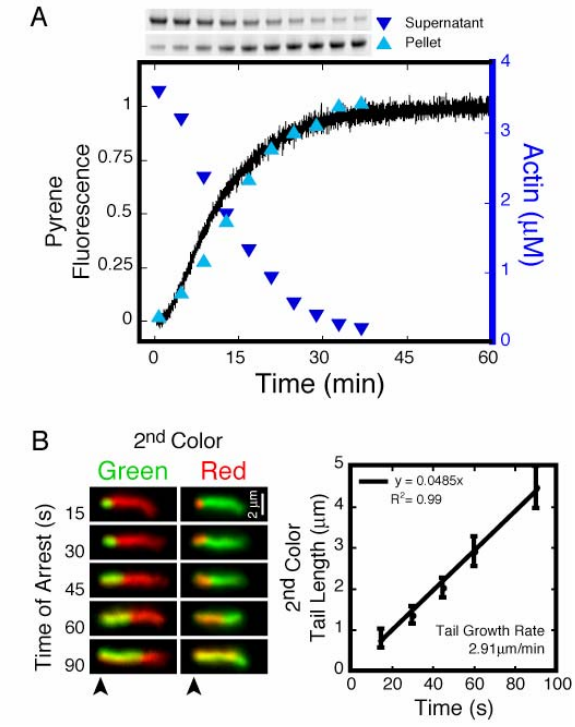

Figure S1. Arresting actin dynamics with Latrunculin B and phalloidin.

A. Used together, Latrunculin B and phalloidin arrest actin dynamics and preserve the distribution of actin between the monomeric and polymeric states. Black trace plots the time course of polymerization of 4 μM actin (5% pyrene labeled), as measured by the increase in pyrene fluorescence. At the indicated time points, aliquots from a parallel polymerization reaction were diluted 1:1 into buffer containing 20 μM each of Latrunculin B and phalloidin. 60 minutes after the start of polymerization, the arrested samples were centrifuged at 360K rcf for 15 minutes. The actin concentration in the supernatants and the resuspended pellets was determined from fluorescently stained SDS-PAGE gels.

B. Latrunculin B/phalloidin treatment arrests Arp2/3-dependent motility and cofilin-dependent network disassembly. Motile comet tails were pulsed with a second color of actin and arrested at the indicated times. Reaction conditions were as described in Figure 1B, with 175 nM Ap2/3 and 168 nM CP. Arrowheads indicate the position of the beads. Increase in length of the second color over time was used to determine the rate of tail growth. Error bars represent standard deviation (average n=39).

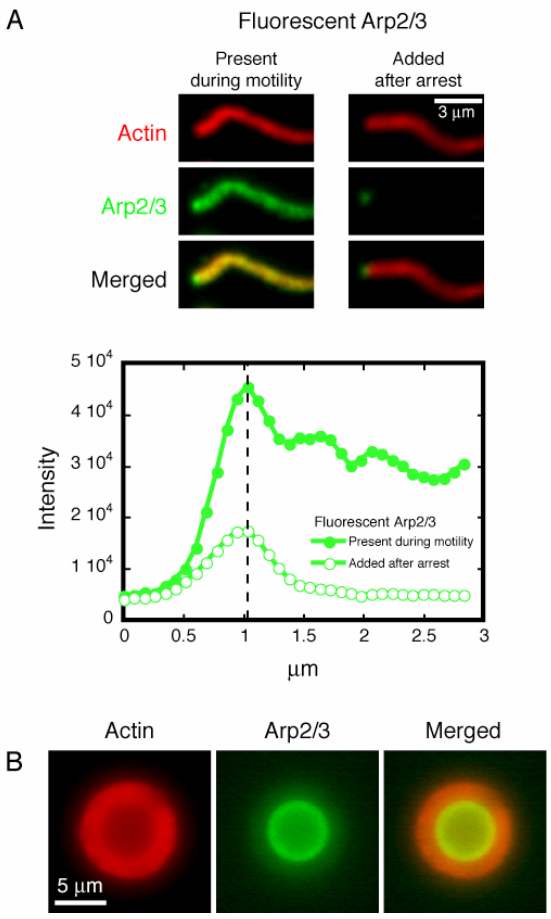

Figure S2. Localization of Arp2/3 in actin comet tails and shells.

A. Nearly all of the Arp2/3 detected in actin comet tails is incorporated into the network through dendritic nucleation at the bead surface. We assembled actin comet tails with Alexa488-labeled (10% of total protein) or unlabeled Arp2/3. 30 minutes after mixing, we arrested motility with Latrunculin B/phalloidin treatment. We then added a matching concentration of Alexa488-labeled Arp2/3 to the tails assembled with unlabeled protein and imaged both reactions using identical settings. Conditions: 7.5 μM actin (5% TMR-labeled), 4 μM cofilin, 3 μM profilin, 175 nM Arp2/3 (with or without 10% Alexa488-labeled fraction), 168 nM CP.

Panels: Representative comet tails assembled with (left) and without (right) Alexa488-labeled Arp2/3. Tails are framed to position the beads (not shown) to the left of each panel. Display limits were set to the same values for each channel.

Graph: Raw pixel intensities along the first two microns of the actin comet tails shown in the green panels are plotted. Dashed line marks the position of the beads.

B. Arp2/3 targets strongly to the bead surface in the absence of ongoing actin assembly. The reaction was Latrunculin B/phalloidin arrested 60 seconds after mixing and incubated with 50 nM Alexa488-labeled Arp2/3. Conditions: 5.8 μm ActA-coated beads mixed with 3 μM actin (5% TMR-labeled), 96 nM Arp2/3, and 84 nM CP.

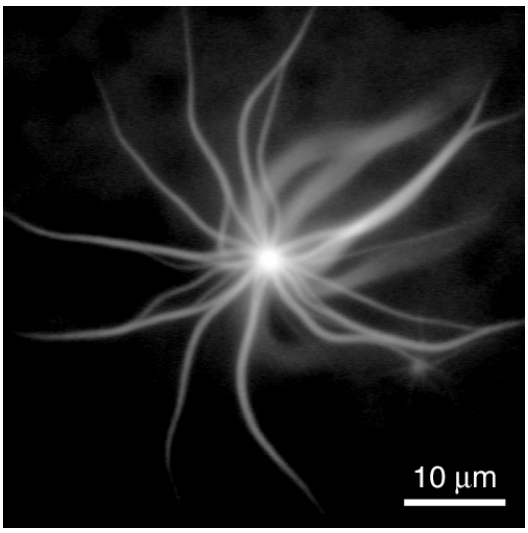

Figure S3. Filament bundling converts actin halos into asters.

Image was acquired 30 minutes after mixing. To display the full length of individual bundles, gamma was set to 2 during brightness and contrast adjustment. Conditions: 0.5 μm ActA[30-170]-coated beads mixed with 7.5 μM actin (5% TMR-labeled) and 50 nM Arp2/3 in the presence of 0.35% methyl cellulose.

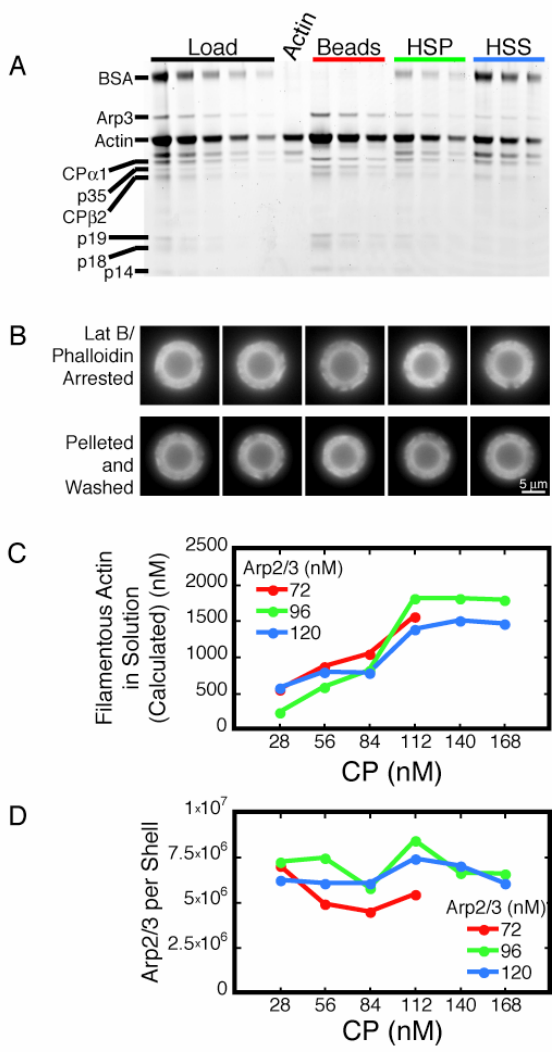

Figure S4. Biochemical analysis of shell growth.

A. Fluorescently stained SDS-PAGE gel of an arrested and fractionated shell growth reaction. Internal standards for each protein were set up using the dilution series of the original reaction (i.e. Load). The composition of the three fractions was determined with a three-point line fit to the standards. The Arp2 and p40 subunits of the Arp2/3 complex migrate too close to actin to be resolved individually. This does not affect the quantification of actin, which was at least twenty times more abundant than Arp2/3 in our experiments.

B. Fractionation and washing do not damage arrested shells.

C. The concentration of filamentous actin not associated with shells increases with [CP]. Values were calculated by subtracting the actin recovered in the shells and the high speed supernatant from the total actin concentration. We noted that amount of actin measured in the high speed pellets actually decreased with increasing [CP]. However, this trend paralleled a decrease in the fraction of starting mass recovered (i.e. (beads+hss+hsp)/input), suggesting that there was a systematic error in material recovery from high speed pellets with increasing [CP].

D. The amount of Arp2/3 recovered in arrested and washed shells does not vary with [CP] or [Arp2/3].

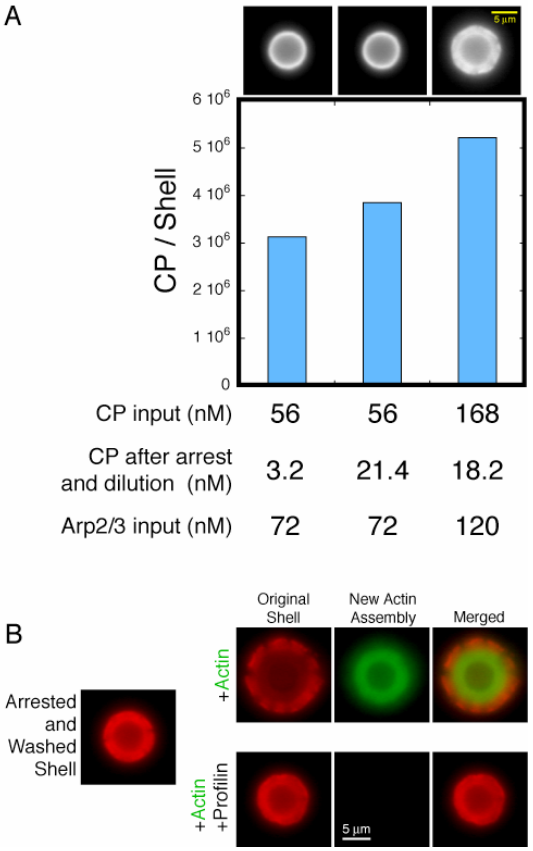

Figure S5. CP recovered from arrested and washed shells is a reliable reporter for the total number of filaments.

A. Non-specific association of CP with actin shells does not account for the increase in CP recovered from shells with increasing starting [CP]. After LatB/phalloidin arrest, we diluted actin shells prepared with low starting [CP] into buffer (left) or buffer with CP (center) to match the total concentration used to prepare shells with high starting [CP] (right). Following a two-minute incubation, all three reactions were processed to determine the protein content in the shells and high speed supernatants as described in the text. Values shown are the average of two independent experiments. Conditions: 5.8 μm ActA-coated magnetic beads, 3 μM actin (5% TMR-labeled).

B. All filaments in an actin shell are capped after LatB/phalloidin arrest. 5.8 μm ActA-coated magnetic beads were mixed with 3 μM actin (5% TMR-labeled), 120 nM Arp2/3, and 168 nM CP to initiate shell growth. The reaction was arrested 60 seconds after mixing and the shells were washed using a magnetic separator. The arrested and washed shells were then mixed with either 3 μM actin (5% Alexa488-labeled) or with 3 μM actin (5% Alexa488-labeled) and 13 μM profilin. This second round of assembly was arrested again 60 seconds after mixing and shells were imaged with fluorescence microscopy. Polymerization in the presence of actin alone is not a result of barbed end elongation but of new filament nucleation by surface-bound Arp2/3, which is inhibited by profilin (Machesky et al., 1999)

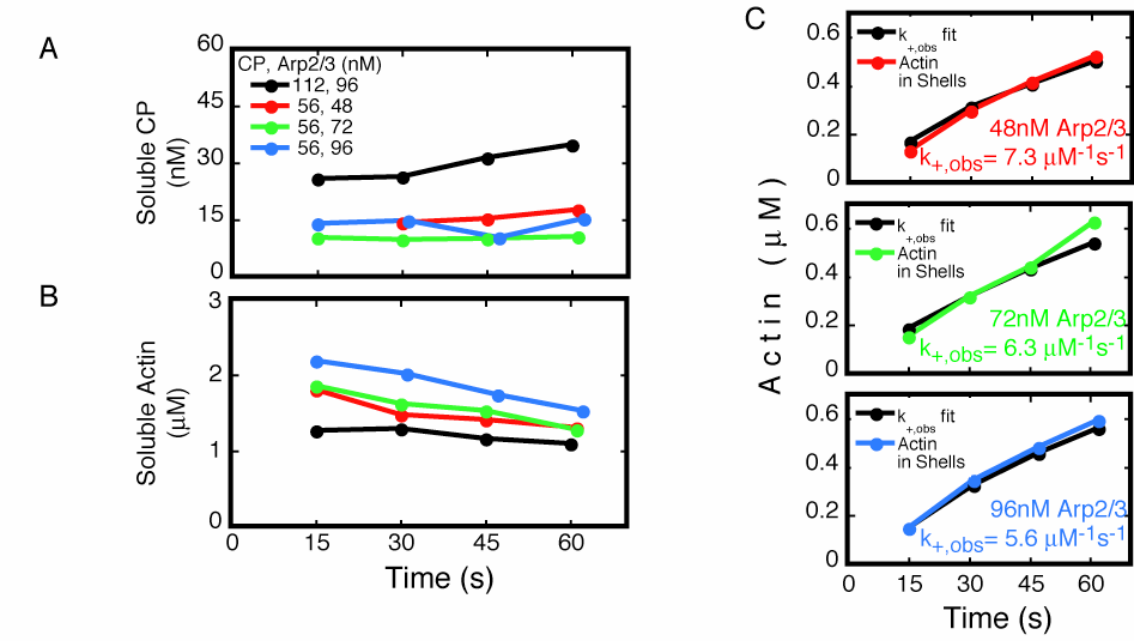

Figure S6. Kinetics of shell growth.
A. Soluble CP concentration for the conditions discussed Figure 5.
B. Soluble actin concentration for the conditions discussed Figure 5.
C. Observed rate of filament elongation does not vary significantly with Arp2/3 concentration. Rates of filament elongation for the conditions discussed in Figure 5 were estimated by comparing the measured actin network assembly with expected assembly, calculated using the measured concentration of monomeric actin and the estimated density of barbed ends (see Supplemental Experimental Procedures for details).

Supplemental References

Co, C., Wong, D. T., Gierke, S., Chang, V., and Taunton, J. (2007). Mechanism of actin network attachment to moving membranes: barbed end capture by N-WASP WH2 domains. Cell *128*, 901-913.

Dayel, M. J., Holleran, E. A., and Mullins, R. D. (2001). Arp2/3 complex requires hydrolyzable ATP for nucleation of new actin filaments. Proc Natl Acad Sci U S A *98*, 14871-14876.

Gordon, D. J., Eisenberg, E., and Korn, E. D. (1976). Characterization of cytoplasmic actin isolated from Acanthamoeba castellanii by a new method. J Biol Chem *251*, 4778-4786.

Kaiser, D. A., Goldschmidt-Clermont, P. J., Levine, B. A., and Pollard, T. D. (1989). Characterization of renatured profilin purified by urea elution from poly-L-proline agarose columns. Cell Motil Cytoskeleton *14*, 251-262.

Machesky, L. M., Mullins, R. D., Higgs, H. N., Kaiser, D. A., Blanchoin, L., May, R. C., Hall, M. E., and Pollard, T. D. (1999). Scar, a WASp-related protein, activates nucleation of actin filaments by the Arp2/3 complex. Proc Natl Acad Sci U S A *96*, 3739-3744.

Otterbein, L. R., Graceffa, P., and Dominguez, R. (2001). The crystal structure of uncomplexed actin in the ADP state. Science *293*, 708-711.

Palmgren, S., Ojala, P. J., Wear, M. A., Cooper, J. A., and Lappalainen, P. (2001). Interactions with PIP2, ADP-actin monomers, and capping protein regulate the activity and localization of yeast twinfilin. J Cell Biol *155*, 251-260.

Pollard, T. D. (1986). Rate constants for the reactions of ATP- and ADP-actin with the ends of actin filaments. J Cell Biol *103*, 2747-2754.

Quirk, S., Maciver, S. K., Ampe, C., Doberstein, S. K., Kaiser, D. A., VanDamme, J., Vandekerckhove, J. S., and Pollard, T. D. (1993). Primary structure of and studies on Acanthamoeba actophorin. Biochemistry *32*, 8525-8533.

Vignjevic, D., Yarar, D., Welch, M. D., Peloquin, J., Svitkina, T., and Borisy, G. G. (2003). Formation of filopodia-like bundles in vitro from a dendritic network. J Cell Biol *160*, 951-962.

Zalevsky, J., Grigorova, I., and Mullins, R. D. (2001). Activation of the Arp2/3 complex by the Listeria acta protein. Acta binds two actin monomers and three subunits of the Arp2/3 complex. J Biol Chem *276*, 3468-3475.